Journal of Solid State Chemistry 182 (2009) 2670–2677

Contents lists available at ScienceDirect

Journal of Solid State Chemistry

journal homepage: www.elsevier.com/locate/jssc

Graphitic carbon nitride $C_6N_9H_3 \cdot HCl$: Characterisation by UV and near-IR FT Raman spectroscopy

Paul F. McMillan [a,*], Victoria Lees [a], Eric Quirico [b], Gilles Montagnac [c], Andrea Sella [a], Bruno Reynard [c], Patrick Simon [d], Edward Bailey [a], Malek Deifallah [a], Furio Corà [a,*]

[a] Department of Chemistry and Materials Chemistry Centre, University College London, 20 Gordon Street, London WC1H 0AJ, UK
[b] Université Joseph Fourier, CNRS/INSU, Laboratoire de Planétologie de Grenoble UMR 5109, Bâtiment D de Physique, BP 53, 38041 Grenoble Cedex 9, France
[c] Laboratoire de Sciences de la Terre, Ecole Normale Supérieure de Lyon, 46 allée d'Italie 69364 Lyon Cedex 7, France
[d] Centre de Recherche sur les Matériaux à Haute Température – CNRS F – 45071 Orléans Cedex 2 et Université d'Orléans, F-45067 Orléans Cedex 2, France

ARTICLE INFO

Article history:
Received 16 March 2009
Received in revised form
29 June 2009
Accepted 2 July 2009
Available online 25 July 2009

Keywords:
Graphitic carbon nitride
UV resonance Raman spectroscopy
FTIR spectroscopy
First principles calculations
DFT calculations

ABSTRACT

The graphitic layered compound $C_6N_9H_3 \cdot HCl$ was prepared by reaction between melamine and cyanuric chloride under high pressure–high temperature conditions in a piston cylinder apparatus and characterised using SEM, powder X-ray diffraction, UV Raman and near-IR Fourier transform Raman spectroscopy with near-IR excitation. Theoretical calculations using density functional methods permitted evaluation of the mode of attachment of H atoms to nitrogen sites in the structure and a better understanding of the X-ray diffraction pattern. Broadening in the UV and near-IR FT Raman spectra indicate possible disordering of the void sites within the graphitic layers or it could be due to electron–phonon coupling effects.

1. Introduction

There is currently great interest in developing the solid state chemistry of novel high-density C–N–H materials that possess useful electronic and mechanical properties. Much of the recent research activity has arisen from the theoretical prediction that dense sp^3-bonded C_3N_4 phases could have extremely low compressibility and high hardness comparable with diamond [1–4]. A large number of experimental studies have been carried out to synthesise such compounds, but reliable characterisation of a bulk C_3N_4 phase with such superhard qualities has remained elusive [5–7]. Other avenues of research have investigated the formation of layered graphitic (C,N) materials that could provide potential precursors to new high-density sp^3-bonded phases as well as having useful properties in their own right. These compounds are now being studied extensively both experimentally and theoretically [4,8–20].

The study of carbon nitride materials prepared by reactions between or decomposition of (C,N)-containing compounds has long constituted an important frontier are between inorganic and organic solid state and molecular chemistry. Liebig first gave the name "melon" to an amorphous solid with an approximate composition near $C_6N_9H_3$ that had been described previously by Berzelius. However, the structural characterisation of a nanocrystalline variety of this material ($[C_6N_7(NH_2)(NH)]_n$) has only been achieved recently [21]. A family of related solid state materials that includes "melem" ($C_3N_{10}H_6$ or $C_6N_7(NH_2)_3$) is now known to exist, with structures based on oligomeric planar units formed by condensation of C_3N_3 (triazine) rings as found in the heterocyclic molecule melamine (2,4,6-triamine-1,3,5-triazine: $C_3N_6H_6$ or $C_3N_3(NH_2)_3$) or triazine itself ($C_3N_3H_3$) [13,21–25] (Fig. 1).

These carbon nitride molecular compounds and solid state materials have important materials applications. They give rise to high-strength refractory plastics including the melamine–formaldehyde series that have been known since the earliest days of carbon nitride chemistry and that are incorporated in polymers to provide flame and heat retardation properties [26]: they also constitute high-energy density materials that can lead to advanced fuels and explosives [27]. Nanomaterials prepared from the condensed heterocyclic systems have useful fluorescence and optoelectronic properties, and graphitic carbon nitrides have been proposed recently as the basis for a new family of H_2O-splitting photocatalysts [10,28].

High-pressure, high-temperature synthesis approaches have been used to prepare relatively well crystallised varieties of graphitic carbon nitride materials by reactions between precursors such as the heterocyclic aromatic compounds melamine and

* Corresponding authors.
E-mail addresses: p.f.mcmillan@ucl.ac.uk (P.F. McMillan), uccacfu@ucl.ac.uk (F. Corà).

0022-4596/$ - see front matter © 2009 Elsevier Inc. All rights reserved.
doi:10.1016/j.jssc.2009.07.030

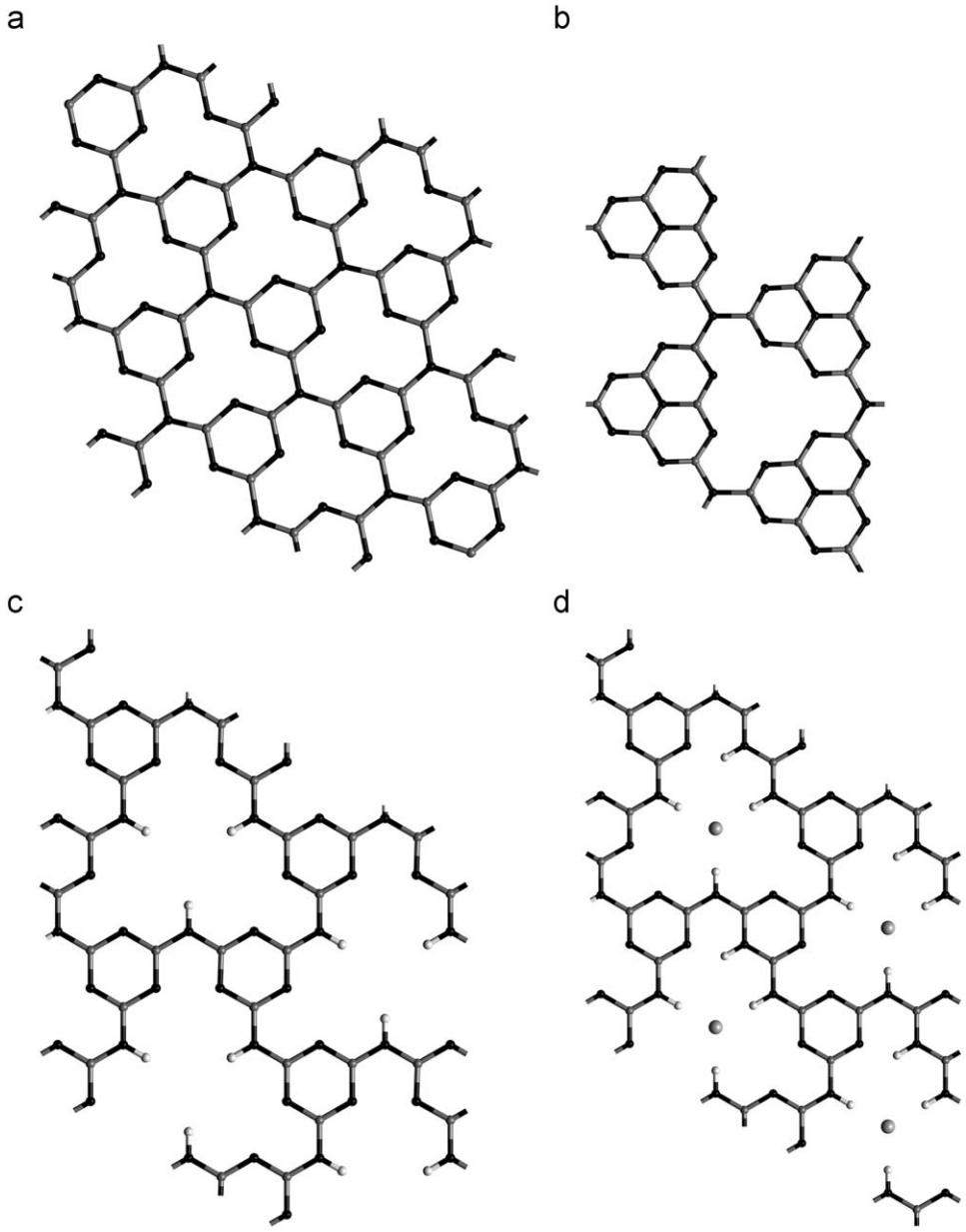

Fig. 1. Structural motifs developed among graphitic sp^2-bonded $C_xN_yH_z$ solids. C atoms are shown in light grey, N atoms are black, and H atoms are shown white. (a) Layers built from triazine C_3N_3 units linked by CNC bonds were proposed for the nanocrystalline g-C_3N_4 structure produced by Kouvetakis et al. [12,16]. The structure contains C_6N_6 "voids" within the graphitic layers. (b) An alternate linking of triazine rings leads to formation of heptazine (C_6N_7) units as found in melem and the presence of larger (C_9N_9) voids in the layered structures of melon and other extended g-C_3N_4 networks [18,19,21,22]. In the case of melon the CNH linkages can be partly hydrogenated. (c) Even larger "voids" ($C_{12}N_{12}$ ring units) are found within $C_3N_9H_3$ layers that form the basis for the graphitic carbon nitride structure proposed by Zhang et al. [17]. Here one half of the CNC groups linking the triazine rings are hydrogenated (N2 atoms). (d) A single layer of the $C_3N_9H_3 \cdot HCl$ structure proposed by Zhang et al. [17]. Note that a Cl atom (or Cl^- ion: large grey) resides within the layer in the centre of the $C_{12}N_{12}$ ring and one additional CNC linkage is hydrogenated, preferentially at the N1 site [30].

cynanuric acid ($C_3N_3Cl_3$) [8,9,14,17]. The layered solid state compounds are formed via lateral condensation or elimination reactions between the planar aromatic rings [19]: e.g.,

$$C_3N_6H_6 + C_3N_3Cl_3 \rightarrow C_6N_9H_3 + 3HCl \quad (1)$$

The pressures used are generally on the order of $P \sim 0.1$–4 GPa at temperatures between 400–600 °C [8,9,14,17,29], much lower than the high P–T conditions used in attempts to produce sp^3-bonded carbon nitride materials.

Demazeau et al. [9] first investigated mixtures of melamine and cyanuric chloride that were reacted at 0.13 GPa and 250 °C: the resulting material exhibited a broad X-ray diffraction peak at ~3.27 Å corresponding to the (002) interlayer reflection of a graphitic (C,N) solid. Chemical analysis also revealed the presence of H and Cl within the material although their role in the structure was not identified. Alves et al. [8] treated melamine in the presence of hydrazine (NH_2NH_2) at 3 GPa and 800–840 °C to obtain a better crystallised product with a larger number of identifiable features in the diffraction pattern. Zhang et al. carried out a systematic study of graphitic (C,N) compounds synthesised from melamine and cyanuric chloride at 1–1.5 GPa and 500–600 °C, and they obtained well-crystallised materials for which structure solutions were proposed following Le Bail and Rietveld refinement of the diffraction data [17,29]. It was indicated that synthesis and crystal growth were optimised in a range bounded by onset of the solid state reaction and thermal

decomposition temperatures, assisted by liquid phase transport within the cyanuric chloride phase, between $P \sim 1.3$–2.2 GPa and $T = 500$–$550\,^{\circ}C$ [29]. Zhang et al. used a combination of bulk chemical analysis and electron energy loss techniques during transmission electron microscopy experiments to establish the composition of the graphitic materials as $C_6N_9H_3 \cdot x$HCl, with $x \sim 1$. These investigations combined with the results of X-ray diffraction analysis thus revealed the presence of Cl atoms within the graphitic (C,N) that were derived from reaction (1) involving the cyanuric chloride precursor: i.e., not all of the HCl component was eliminated but was incorporated within the structure. The Cl atoms were proposed to occupy voids within the graphitic (C,N) layers (Fig. 1). Based on the results of ^{13}C NMR and FTIR spectroscopy, Zhang et al. suggested that the additional H atoms associated with incorporation of the HCl component in the structure should be attached to the N(1) nitrogen atoms involved in the triazine rings rather than to the N(2)H groups bridging between triazine units and forming the $C_{12}N_{12}$ voids within the structure (Fig. 1). Our recent density-functional theoretical calculations (DFT) indicate that this interpretation is correct [30]. In the present work, we show that the results of the first principles DFT calculations allow us to refine further details of the structure and achieve a better understanding of the X-ray diffraction data. In our new study we also used UV and near-IR Fourier transform Raman spectroscopy to gain new insights into the structural ordering and phonon–electron interactions within the graphitic layered C,N compounds.

2. Experimental methods

Melamine ($C_3N_6H_6$) and cyanuric chloride ($C_3N_3Cl_3$) were obtained from Aldrich and used without further purification: they were stored in an Ar-filled dry box (<10 ppm O_2/H_2O) that was used for all subsequent sample manipulations including loading into the high-pressure capsules for synthesis experiments. For high-*P,T* syntheses we used a non end-loaded piston cylinder device obtained from Depths of the Earth Co, Arizona, USA. In a typical run a 1:2 mixture of melamine:cyanuric chloride was pressed into a pellet and loaded into a preformed Pt capsule (5 mm outer diameter) that was sealed by crimping inside the dry box. The sample weight was ~250 mg. The loaded capsule was then placed inside a graphite heater assembly with a NaCl outer sleeve that acted as the pressure-transmitting medium. Syntheses were carried out at pressures ranging between 0.5 and 1.5 GPa at temperatures of 500 and 600 °C measured by a $W_{97}Re_3$–$W_{75}Re_{25}$ thermocouple for 15 h. Following decompression to ambient conditions we detected evolution of HCl gas on opening the capsule, as expected from the formal synthesis reaction (1). However, subsequent chemical and structural analysis revealed that substantial Cl remained incorporated within the graphitic structure, as already indicated by Demazeau et al. and Zhang et al. [9,17].

The recovered yellow–brown solid was washed with distilled H_2O, ethanol and acetone to remove $Pt(NH_3)_4Cl_2$ that typically formed by reaction with the capsule material during the high-*P,T* synthesis experiment as well as any unreacted starting materials; the product was then dried at 130 °C [17,29]. SEM investigations indicated formation of a layered solid state material, with particle sizes ranging between ~0.1 and 0.5 μm. Bulk chemical analyses were carried out at UCL. The C:N:H determinations gave an average formula $C_6N_{9.0\pm0.5}H_{6.5\pm1.5}$ consistent with the stoichiometry found previously by Zhang et al. [17,29]. We could not achieve a reliable determination of the Cl content in our experiments. We were forced to combine samples produced from several synthesis runs and we found the Cl contents to be variable and generally much higher than expected for a composition

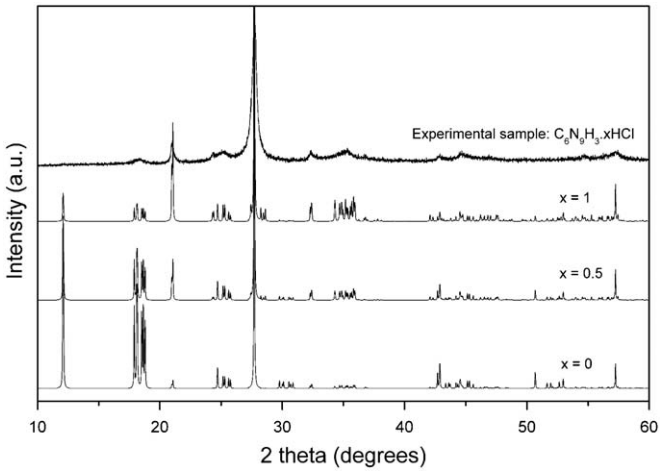

Fig. 2. Top: experimental powder X-ray diffraction pattern for the layered graphitic $C_6N_9H_3 \cdot x$HCl as prepared in this study following washing. Bottom: calculated patterns using different Cl site occupancies predicted from DFT calculations (assuming *P*1 symmetry) [30]. The calculated patterns best match the experimental diffraction data for $x = 1$.

$C_6N_9H_3 \cdot$HCl. We believe that this result is due to incorporation of $Pt(NH_3)_4Cl_2$ species that are formed as byproducts of the reaction and that were not fully removed by washing and were included in the combined samples sent for chemical analysis. Our analysis of the X-ray diffraction results presented below combined with DFT theoretical predictions of the X-ray patterns were consistent with the $C_6N_9H_3 \cdot$HCl formulation, and we presumed that the chemical composition analyses presented previously were correct [17,29]. The samples were examined by powder X-ray diffraction using a Bruker D4 diffractometer and Cu*K*α ($\lambda = 1.5418$ Å) radiation at UCL. The relative intensities observed in the powder X-ray diffraction pattern matched those expected for a graphitic layered $C_6N_9H_3 \cdot x$HCl material with $x = 1$ (Fig. 2).

Raman spectroscopy is well established as a useful technique for studying the structure and interactions between vibrational and electronic excitations in graphitic carbon-based materials [31–35]. However, no Raman spectra have been reported to date on the carbon nitride compounds obtained from high-*P,T* synthesis, because of the strong fluorescence produced by these materials under visible excitation that obscures the weak Raman scattering. In our study we first attempted to obtain Raman spectra with laser excitation throughout the visible range (787–325 nm) using home-built [36] and commercial (Renishaw) micro-Raman systems at UCL. All of these experiments resulted in intense photoluminescence that obscured the Raman spectra, even when excited into the UV range (Fig. 3). Previous studies of similar layered and nanocrystalline C_xN_y compounds have also reported intense photoluminescence when excited by visible radiation [10].

Molecular, oligomeric and solid-state aromatic systems including those based on C,N heterocycles often exhibit strong fluorescence when excited by visible radiation due to π–π^* and other electronic transitions. However, excitation with UV radiation above the range of most of the electronic transitions could result in the appearance of useful Raman spectra. Here we explored the use of UV excitation in the 240–250 nm range to record the first series of Raman spectra for $C_6N_9H_3 \cdot$HCl as well as other graphitic C_xN_y compounds known as "tholins", and that are important in planetary physics and atmospheric research [37] (Fig. 4). In a first series of runs, the solid state samples were excited using 244 nm radiation from a frequency-doubled Ar^+ laser using a Jobin Yvon-Horiba LabRam UV Raman system installed in the Laboratoire des Sciences de la Terre at ENS Lyon. In micro-beam experiments the

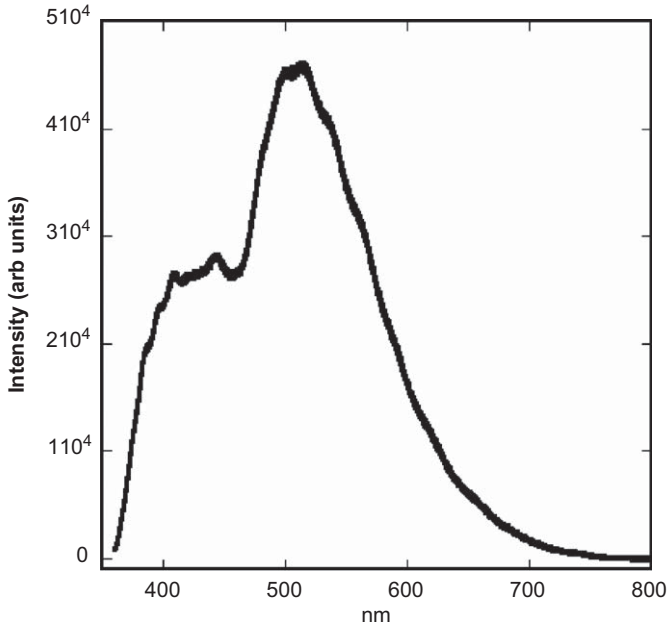

Fig. 3. Room temperature photoluminescence spectrum of graphitic $C_6N_9H_3 \cdot HCl$ produced via high-*P,T* synthesis from heterocyclic aromatic precursors excited using 325 nm laser excitation. Raman peaks appear as weak features on the high energy side of the main fluorescence peak, shifted by ~1000–1800 cm^{-1} from the exciting line.

incident laser was focused on the sample via a UV microscope objective and spectra obtained in a back-scattering geometry. The sample area illuminated was 4–5 μm in diameter. During preliminary experiments conducted with higher incident laser powers we observed time-dependent changes in the spectra that could be attributed to sample degradation during UV laser irradiation. In subsequent studies we reduced the laser power to only a few mW incident on the sample and no longer observed any such spectral changes: we believe that those results correspond to the true UV Raman spectra of the graphitic $C_6N_9H_3 \cdot HCl$ compound (Fig. 4). To further confirm that no sample degradation had taken place we also carried out additional measurements in the LEPMI-CMTC Laboratory at INPG Grenoble using 229 nm laser excitation with the sample mounted on a rotating stage to dissipate any heating effects during the experiment. The spectrometer was a Jobin Yvon T64000 instrument equipped with an 1800 g/mm grating. The results were identical with those obtained at ENS Lyon using low incident laser power.

During UV excitation of carbonaceous graphitic materials including C_xN_y compounds with substantial sp^2 bonding and low-energy electronic excitations, it is now well known that the Raman spectra can exhibit significant resonant enhancement of vibrational contributions from structural species that are present even in small concentrations, and that changes in relative band intensity and lineshapes can occur as a result of coupling between vibrational and electronic excitations [31–35,38]. In our work we further investigated the Raman spectra of our samples obtained using near-IR (1064 nm) excitation provided by a Nd^{3+}:YAG laser in a Fourier transform (FT) Raman experiment using a Bruker IFS88 spectrometer at CRMHT-CNRS Orléans (Fig. 4). For the FT-Raman experiments the sample was pressed into a disc in an Al holder and spectra were taken on 100 μm spots. The instrumental resolution was 4 cm^{-1}.

Theoretical calculations of various $C_6N_9H_3$ and $C_6N_9H_3 \cdot HCl$ layered materials and graphitic compounds were carried out using periodic boundary conditions within the local density

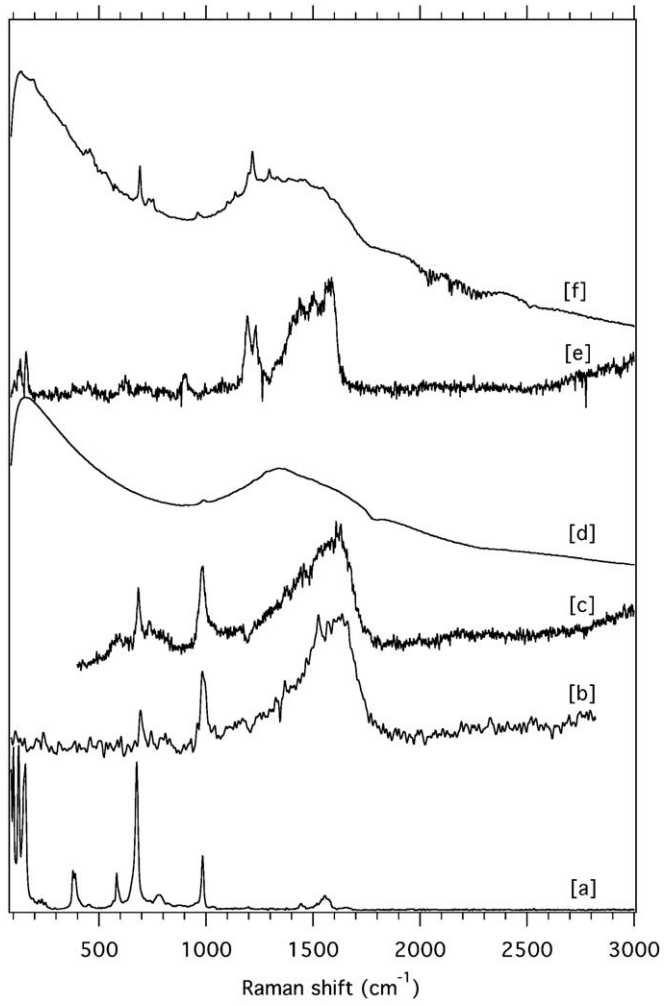

Fig. 4. UV (244 or 229 nm excitation) and FT Raman spectra (1064 nm excitation) obtained for graphitic and oligomeric C_xN_y samples at ENS Lyon, LEPMI-CMTC Grenoble and CNRS-CRPHT Orléans: (a) *s*-triazine (1064 nm); (b) *g*-$C_6N_9H_3 \cdot HCl$ (229 nm: rotating stage); (c) *g*-$C_6N_9H_3 \cdot HCl$ (244 nm); (d) *g*-$C_6N_9H_3 \cdot HCl$:1064 nm; (e) melon ($C_6N_7(NH_2)(NH)$): 229 nm excitation: rotating stage; (f) melon; 1064 nm excitation.

approximation (LDA) of density functional theory (DFT) using the plane wave code CASTEP [30,39]. We used ultra-soft pseudopotentials for C, N, H and Cl atoms and optimised the cut-off energy (450 eV) and k-point grid size ($3 \times 3 \times 4$) from single energy point calculations. Further details of the calculations are presented elsewhere [30,39].

3. Results and discussion

3.1. X-ray diffraction and structural modelling

The samples prepared in this study had X-ray diffraction patterns that were similar to those reported previously by Zhang et al. for graphitic $C_6N_9H_3 \cdot HCl$ [17,29] (Figs. 2, 6). Although the X-ray patterns reveal a relatively well crystallised material the lines remain broadened compared with well-ordered bulk crystals indicating the presence of substantial structural disorder within the graphitic carbon nitride layers, or that the samples are nanocrystalline. Our results indicate that both disorder-induced broadening and nanoparticle size-effect (Scherrer) broadening are likely to be present. Zhang et al. [17] fit their original data to a layered hexagonal ($P6_3/m$) structure using a combination of Le

Bail extraction and Rietveld refinement techniques. The underlying $C_6N_9H_3$ unit has a structure based on stacking of (C,N) graphene planes (Figs. 1, 5). A fully ordered structural model of this type contains alternating sp^2-bonded C and N atoms forming triazine (C_3N_3) rings that are linked by (NH) units to form voids ($C_{12}N_{12}$) within the graphitic layers (Fig. 1). The large voids are occupied by Cl^- ions and additional H^+ species are attached to N2 atoms within the $C_6N_9H_3 \cdot HCl$ structure; the Cl component found within the structure results from the cyanuric chloride used in the synthesis reaction (1). It is possible that not all of the void sites within the layers are fully occupied, resulting in potential formulations such as $C_6N_9H_3 \cdot xHCl$ ($0 \leq x \leq 1$). However, from their determinations of the chemical composition using bulk and EELS techniques, Zhang et al. concluded that a structure in which all available sites within the layers were occupied by Cl atoms provided the best solution [17,29]. Our analysis of the X-ray diffraction results agrees with that conclusion. We calculated the powder diffraction patterns for various graphitic materials $C_6N_9H_3 \cdot xHCl$ with x values ranging from 0 to 1 and found best agreement with the observed pattern for $x = 1$ (Fig. 2).

The occurrence of both relatively narrow and broad peaks in the X-ray diffraction pattern cannot be explained by the $P6_3/m$ structural model proposed by Zhang et al. Our theoretical calculations indicate that the N–H bonding pattern combined with correlated displacements of the Cl^- ions away from the ring centre cause lowering of the crystal symmetry. Structurally distinct N atoms are defined as those involved in triazine ring formation (N1) and those providing NH linkages between the C_3N_3 units (N2). The additional protons provided by the HCl incorporation are located at the N1 sites (Fig. 1) [17,30]. This then results in disordering within the layers because each additional H atom is attached to one of the six possible N1 sites. In addition, the extra $\delta+$ charge at each protonated N1 site causes a slight shift of the Cl^- ion from the centre of the large void. We recently examined these effects via DFT-LDA calculations to predict the powder X-ray diffraction pattern of a distorted version of the Zhang et al. model, assuming only $P1$ space group symmetry (Fig. 6). The $P6_3/m$ structure determined by Zhang et al. had cell parameters $a = b = 8.4379$ Å; $c = 6.4296$ Å (α, $\beta = 90°$); our distorted $P1$ version of the structure was optimised with $a = 8.372$ Å, $b = 8.370$ Å, $c = 6.230$ Å; $\alpha = 89.68°$; $\beta = 92.56°$ [30]. The proposed structural distortions result in a better interpretation of the observed powder X-ray diffraction profile, in that reflections that are isolated or lie close together in the $P1$ structure (e.g., 110; 120; 002; 120) correspond to narrow

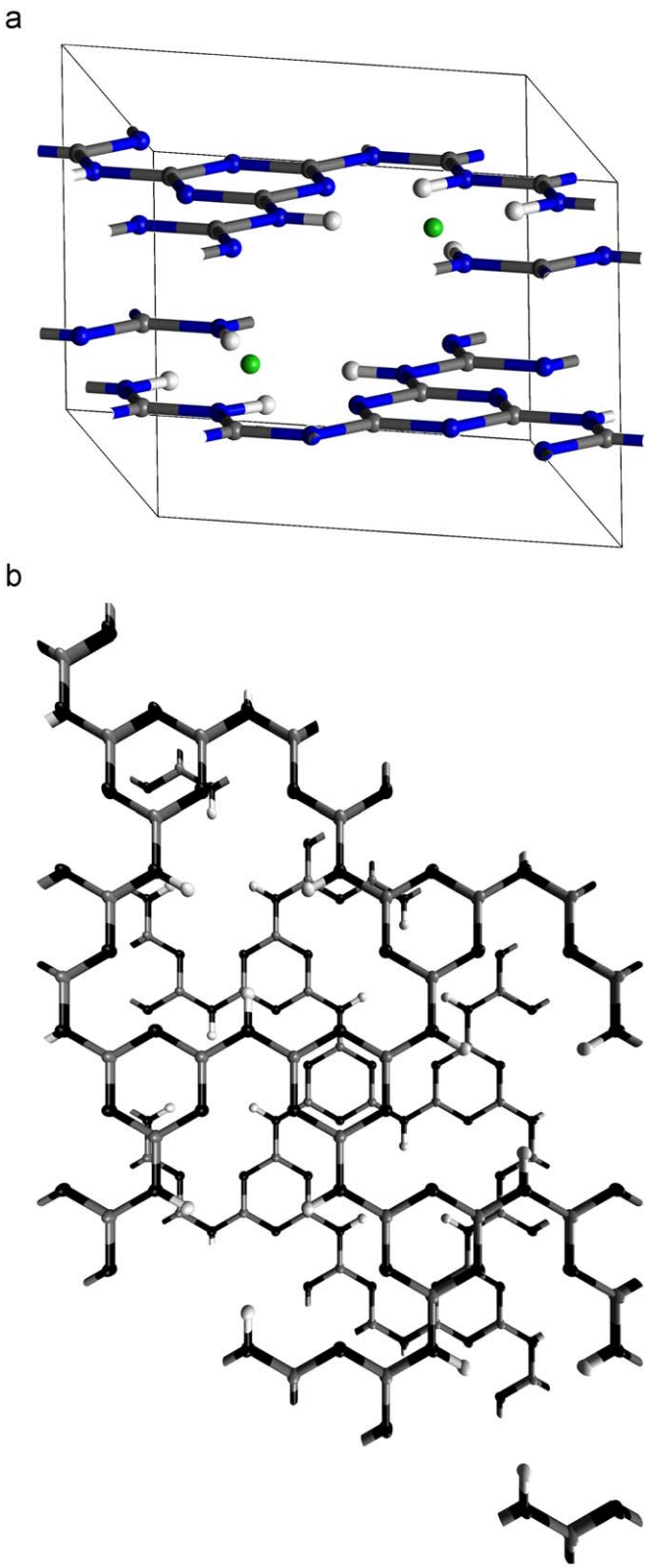

Fig. 5. Stacking of the layers in the graphitic $C_6N_9H_3 \cdot HCl$ structure. The attachment of additional H atoms to the N2 atoms decorating the $C_{12}N_{12}$ rings is not shown here for clarity.

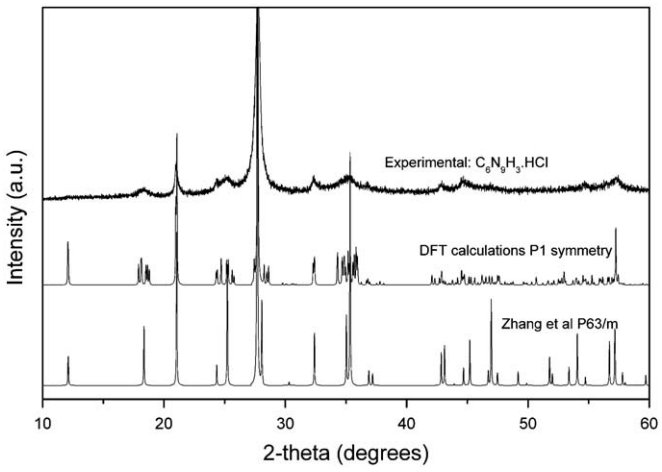

Fig. 6. Powder X-ray diffraction pattern of graphitic $C_6N_9H_3 \cdot HCl$ compared with the $P6_3/m$ structure proposed by Zhang et al. [17] (top) and the lower diagram indicates the diffraction peaks calculated for a structural model with $P1$ symmetry that assumes an ordered H–N attachment arrangement to the N1 nitrogens and with Cl atoms moved slightly off centre within their sites accordingly [30]. In the true overall structure it is likely that the N1–H attachment and Cl displacements occur in a disordered manner within each layer.

reflections in the experimental pattern, whereas groups of reflections with approximately equal intensities over a range of 2Θ values give rise to broad bands (e.g., at 17.5–19.5°, 24–26° and 34–36°) (Fig. 6). We did not attempt further refinement of the structure from the experimental data for several reasons. First, our experimental data were already comparable in quality to those analysed by Zhang et al. [17,29]. Reducing the symmetry and introducing new structural variables could certainly improve the fit parameters, but there would be no statistical significance to the result. Also our analysis indicates that the local distortions caused by the H incorporation pattern is likely to be present in a disordered manner between different unit cells [30].

3.2. IR spectra

The IR spectrum of $C_6N_9H_3 \cdot HCl$ contains sharp peaks throughout the skeletal region between 1000 and 1700 cm^{-1} due to C–N stretching and bending vibrations within the heterocyclic aromatic ring system [40,41] (Fig. 7). X-ray amorphous "tholins", CN_x and C_xN_y polymers only contain broad bands throughout this range [42,43]. However, nanocrystalline melon with a well defined crystal structure determined by electron diffraction has a similar series of sharp IR peaks [21]. Two distinct groups of peaks are observed in the IR spectrum for $C_6N_9H_3 \cdot HCl$ at 666, 636 and 630 cm^{-1}, and at 832, 817 and 782 cm^{-1}. In their theoretical study of *s*-triazine Larkin et al. [40] assigned modes at 748 and 675 cm^{-1} to out-of-plane and in-plane bending vibrations of the C_3N_3 ring. A similar interpretation was proposed by Wang et al. [41] for IR- and Raman-active bands occurring for melamine ($C_3N_6H_6$), although these authors also found significant contributions from $-NH_2$ torsional motions in that spectral region. In the high frequency range, we observe broad bands with principal maxima at 3024 and 2754 cm^{-1}, with a shoulder present at ~2900 cm^{-1} (Fig. 7). Zhang et al. observed similar features [17]. These bands can be assigned to stretching vibrations of H-bonded N–H species.

Melamine and melem both contain sharp high frequency peaks at above 3400 cm^{-1} due to N–H vibrations that are not involved in H-bonding. Spectra of these materials recorded in the solid state also contain broader bands at lower wavenumber (3000–3350 cm^{-1}) that are assigned to N–H species involved in H-bonding; these broad features do not appear in gas phase or matrix isolation experiments on melamine molecules [17,22,41]. Only broad bands at 3000–3500 cm^{-1} are observed in spectra of amorphous hydrogenated CN_x materials and tholins [42,43]. In the case of melamine, the H-bonding occurs between the molecular units, whereas for oligomers and graphitic materials built from condensation of triazine rings internal N–H…N bonding can also occur across portions of the $C_{12}N_{12}$ voids [17,30]. The 3024 cm^{-1} band of $C_6N_9H_3 \cdot HCl$ is assigned to N–H stretching of protonated N2 sites that can engage in H-bonding interaction with the Cl^- ion located in the centre of the $C_{12}N_{12}$ ring [17].

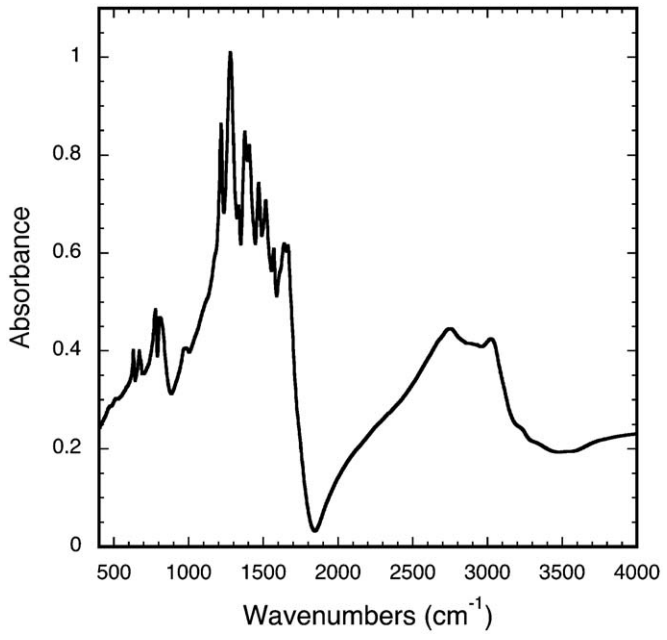

Fig. 7. FTIR transmission spectrum of graphitic $C_6N_9H_3 \cdot HCl$ prepared as a KBr disc under moisture-free conditions in a glove box.

The frequency of the 2750–2780 cm^{-1} band in the IR spectrum of $C_6N_9H_3 \cdot HCl$ is anomalously low. The possibility that it might be assigned to C–H stretching was ruled out by ^1H–^{13}C cross-polarisation NMR experiments [17]. It has been proposed that this band is due to N–H stretching of the bridging imido groups with a potentially strong intramolecular H-bonding interaction occurring with an adjacent unprotonated N1 atom [17]. IR spectra of related materials have been reported by Komatsu [23] and by Lotsch et al. [21], who also carried out a detailed characterisation of nanocrystalline carbon nitride phases using electron diffraction and solid state NMR techniques.

3.3. Raman spectroscopy

Our first attempts to obtain Raman spectra using laser excitations ranging throughout the visible to UV wavelengths (i.e., 785, 514.5, 488, 325 nm) were unsuccessful because of strong photoluminescence that obscured the Raman spectrum (Fig. 3). UV Raman spectra free from fluorescence effects were first obtained using 244 nm excitation at ENS Lyon and then with 229 nm excitation using a rotating stage system at IPNG Grenoble (Fig. 4). Later we also obtained Raman spectra using near-IR (1064 nm) excitation in Fourier transform (FT-Raman) experiments at CNRS Orléans: the results were reproduced in separate experiments using a similar Bruker instrument at Nottingham University.

The UV Raman spectra were dominated by a broad asymmetric band at 1200–1700 cm^{-1} due to C–N stretching vibrations, that resembles the "G" and "D" band profiles observed for structurally disordered graphitic carbons and other (C,N) layered materials [31,33,35,44]. We found it surprising that such a "disordered" Raman band profile should be observed for graphitic $C_6N_9H_3 \cdot HCl$ that exhibits a highly crystalline X-ray diffraction pattern. That result is discussed further below. Two sharp peaks were observed at 690 and 980 cm^{-1} in the UV Raman spectra (Fig. 4). These can be interpreted by comparison with *s*-triazine and melamine that provide simple heterocyclic molecules containing the C_3N_3 triazine ring species with Raman and IR spectra that have been assigned using empirical and *ab initio* force field calculations [17,22,40–42]. The symmetric breathing vibration of N atoms within the C_3N_3 ring is uncoupled from other vibrational modes and it gives rise to a strong Raman band at 970–1000 cm^{-1} for both molecules (Fig. 4). We thus assign the 980 cm^{-1} UV Raman peak of graphitic $C_6N_9H_3 \cdot HCl$ to the symmetric N-breathing mode of triazine rings within the structure. The second sharp peak in the UV Raman spectra at 690 cm^{-1} corresponds to a strong Raman feature observed for *s*-triazine and melamine, due to a doubly degenerate mode involving in-plane bending vibrations of the CNC linked triazine linkages in these molecules [40,42] (Fig. 4). No bands were observed in the 2000–2500 cm^{-1} region in either Raman or FTIR spectra, indicating the absence of any triply bonded C≡N units or N=C=N groups within the structure [43,45–47].

It is known that the UV Raman spectra of carbonaceous materials containing aromatic π-bonding can be significantly affected by resonance effects [32,34,37,38,48]. These can greatly enhance the contributions from minor species within a sample. The HOMO–LUMO gap mainly due to $\pi-\pi^*$ transitions in polycyclic aromatic systems varies with wavelength and vibrations of the C_3N_3 rings within a C,N graphitic system would be expected to be most sensitive to a UV Raman experiment. We thus obtained FT-Raman spectra using 1064 nm laser excitation. A very weak feature appears in the FT-Raman spectra near 980 cm^{-1}, that we attribute to the N-symmetric stretching of C_3N_3 rings in the structure, as for the UV Raman data. The FT-Raman spectra showed a broad principal band at 1300–1400 cm^{-1} with shoulders at ~1600 and 1800–2000 cm^{-1} occurring in the general range of C–N stretching vibrations. The peak shape and the position of its maximum differ from those recorded using UV Raman spectroscopy: that result agrees with the excitation wavelength-dependent dispersion among the G and D peaks of amorphous carbons and C,N graphitic materials documented by Ferraro et al. [31–35].

It was noted above that the observation of such a broad and asymmetric Raman principal band was unexpected for the apparently highly crystalline samples. One possibility is that the materials are actually disordered within the layers in a way that affects the phonon propagation but does not significantly perturb the X-ray diffraction pattern. We have already noted that the N–H attachment to the triazine N1 atoms is likely to occur in a disordered manner and there are small shifts of the Cl atoms away from the centres of the $C_{12}N_{12}$ rings. Another possibility is that the $C_{12}N_{12}$ and C_3N_3 rings could be distributed in a disordered manner within the layers resulting in a loss of translational order for propagation of phonons within the layers. The FT-Raman spectrum exhibits a broad feature rising towards the laser line at low frequency. It is cut off by the laser bandpass filter at ~60 cm^{-1}. The intensity of this feature relative to higher frequency Raman bands in Stokes vs anti-Stokes spectra, as well as the changes in Stokes vs anti-Stokes spectra at low T, confirms that the band has a vibrational origin in the low frequency density of states spectrum, that is normally only activated for amorphous solids [49–53] (Fig. 8). However those effects should result in analogous peak broadening in the FTIR spectrum, that is not observed (Fig. 7). Another possibility is that the broad Raman bands observed with both UV and near-IR laser excitation result from electronic–vibrational coupling effects, as have been documented for other carbonaceous and graphitic C,N materials [31–35]. This result must be explored in future studies.

Very recently, Zinin et al. have reported UV Raman spectra and near-IR Raman spectra (using 785 nm excitation, at a wavelength considerably shorter than the 1064 nm excited FT Raman spectra recorded here) of a graphitic carbon nitride material prepared by a solvothermal reaction between cyanuric chloride and $NaNH_2$ in benzene, or by a solid state reaction between C_3N_3Cl and Li_3N [54]. The results obtained by these workers were generally similar to the data obtained here for the well crystallised g-$C_6N_9H_3 \cdot HCl$ material. The UV Raman data showed a sharp peak at 691 cm^{-1} that is likely the same as that observed in our study: additional sharp features occur just above 1000 cm^{-1} that could also be due to C_3N_3 rings present in the structure. However, as noted above, the likely resonant nature of the UV Raman spectroscopy experiment means that only a very small fraction of the total sample might be contributing to these features. In the 1500–1700 cm^{-1} region, a broad asymmetric band was observed similar to that recorded for our samples, but Zinin et al. do not consider that this is related to the G band spectrum of graphitic carbon materials. Instead they suggest it could be due to C=N stretching vibrations within the g-C_3N_4 rings. They do not explore the possibility of structural disorder or electron-phonon coupling

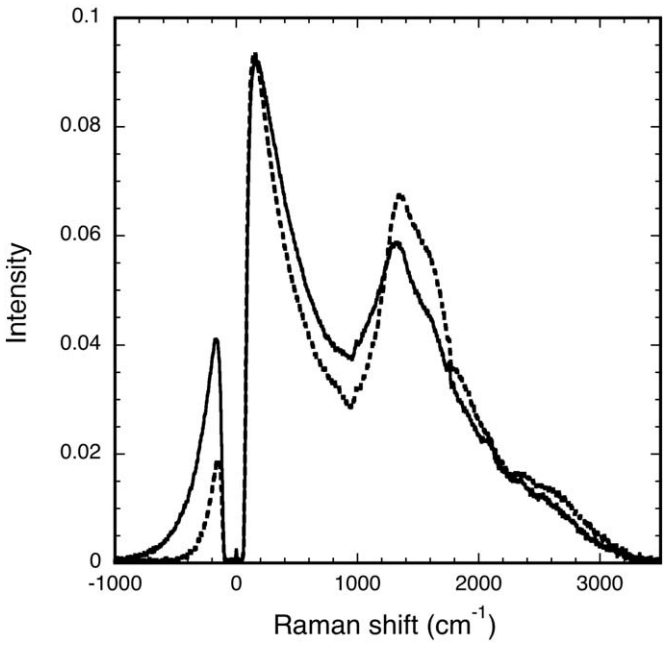

Fig. 8. FT Raman spectra of graphitic $C_6N_9H_3 \cdot HCl$ with 1064 nm excitation at ambient T (300 K: solid line) and at low T (~80 K: dashed).

in their interpretation of the spectra. They also noted that the Raman spectra obtained with 785 nm excitation were quite different to the UV Raman spectra, with one or two broad bands with a few sharp peaks superimposed on a continuous background descending from ~450 cm^{-1} (they did not obtain spectra in the low frequency range, nor did they study Stokes vs anti-Stokes spectra as presented here).

As discussed above in relation to our own results, it is quite likely that a simple interpretation and comparison between UV and near-IR Raman data is not possible in terms of the graphitic nitride structure alone, and that electronic effects must be taken into account at several levels. First, the resonance enhancement of the Raman signature from a small proportion of structural elements within the structure especially with UV irradiation must be considered, and this will change as a function of the local and extended electronic structure that varies as a function of heterocyclic ring size and connectivity. Next, electron–phonon coupling will cause broadening of vibrational Raman bands and also result in dispersion of the principal features, as demonstrated for graphitic carbon and C_xN_y materials [31–35]. Finally, the possible effects of structural disorder such as an assemblage of different ring sizes present and co-polymerised with the graphitic layers, that would not be detected by an X-ray diffraction experiment, could cause broadening and the relaxation of normal FTIR and Raman selection rules, along with the appearance of a "boson" peak in the Raman spectra at low frequency. All of these features must be investigated in future studies, for samples that are structurally well characterised. The combination of Raman data obtained with different excitation wavelengths along with theoretical investigations of the electronic and vibrational properties will lead to a new level of understanding of the structure of the various families of graphitic carbon nitride materials.

5. Conclusions

We have reproduced the synthesis of a highly crystalline C,N graphitic compound $C_6N_9H_3 \cdot HCl$ by reaction between melamine and cyanuric chloride under high pressure–high temperature

conditions [17]. The X-ray diffraction pattern exhibits a series of well-defined peaks that previously permitted establishment of a structural model for the layered graphitic material [17,29]. The diffraction pattern contains families of both broad and relatively narrow peaks that were not explained by the preliminary structural model. From our *ab initio* DFT calculations and consideration of the H incorporation pattern within the graphene layers we find that the local arrangement of N–H bonds cause distortions within the planar lattice and that these are likely to be disordered. Predictions of the distorted structure result in families of X-ray diffraction peaks that explain the pattern of broad and narrow reflections in the observed data. We investigated the structure of the layered graphitic compound using UV Raman and also FT-Raman spectroscopy with near-IR excitation. Previous attempts to obtain conventional Raman spectra with excitation throughout the visible spectrum had been unsuccessful due to strong fluorescence of the sample. The UV Raman spectrum was dominated by a strong, broad asymmetric feature similar to that observed for amorphous carbon and highly disordered C-graphitic structures. Sharp peaks observed at lower wavenumber are due to symmetric stretching vibrations of C_3N_3 triazine rings. The UV Raman spectra might be dominated by resonance Raman effects and the observed spectra could represent only a small fraction of the structural species present within the sample. We obtained FT-Raman spectra with near-IR (1064 nm) at ambient and low temperature to examine this possibility. The main Raman band moved to lower wavenumber but remained broad. The results indicate either that disorder occurs within the C,N graphitic layers, that could be correlated with disordering in the linkage formation between C_3N_3 triazine units and resulting dispersion in the void sizes within the layers, or that electron–phonon coupling effects result in extreme broadening of Raman active modes upon excitation across a wide range of the optical spectrum. Our present results do not permit any further conclusion. The IR spectra contain sharp peaks throughout the skeletal (C,N) stretching range that are consistent with vibrations of condensed heterocyclic aromatic ring units. The N–H stretching vibrations are broadened and shifted to low frequency by H-bonding effects, including NH…Cl^- bonding and intramolecular NH…N bonding across short distances within the $C_{12}N_{12}$ voids within the graphitic layers.

Acknowledgments

This work was supported by EPSRC Grants GR/T00757 and EP/D504782 to PFM. Work by E. Quirico and colleagues in Grenoble was funded by the Centre National d'Etudes Spatiales (CNES). We thank A. Crisci (LEPMI/INPG-Grenoble, France) for his assistance during 229 nm UV Raman experiments and A. Salamat (UCL) for assistance with drafting X-ray diffraction figures.

References

[1] M.L. Cohen, Phys. Rev. B 32 (1985) 7988.
[2] M.L. Cohen, A.Y. Liu, Science 245 (1989) 841–842.
[3] A.Y. Liu, M.L. Cohen, Science 245 (1989) 841.
[4] D.M. Teter, R.J. Hemley, Science 271 (1996) 53.
[5] J. Haines, J.M. Léger, G. Bocquillon, Ann. Rev. Mater. Res. 31 (2001) 1–23.
[6] E. Horvath-Bordon, R. Riedel, A. Zerr, P.F. McMillan, G. Auffermann, Y. Prots, R. Kniep, P. Kroll, Chem. Soc. Rev. 35 (2006) 987–1014.
[7] S. Veprek, J. Vac. Sci. Technol. A 17 (1999) 2401–2419.
[8] I. Alves, G. Demazeau, B. Tanguy, F. Weil, Solid State Commun. 109 (1999) 697.
[9] G. Demazeau, H. Montigaud, B. Tanguy, M. Birot, J. Dunogues, Rev. High Pressure Sci. Technol. 7 (1998) 1345.
[10] Q. Guo, Q. Yang, L. Zhu, C. Yi, S. Zhang, Y. Xie, Solid State Commun. 132 (2004) 369–374.
[11] T. Komatsu, J. Mater. Chem. 11 (2001) 802–805.
[12] J. Kouvetakis, A. Bandari, M. Todd, B. Wilkens, N. Cave, Chem. Mater. 6 (1994) 811.
[13] J.E. Lowther, Phys. Rev. B 59 (1999) 11683–11686.
[14] H. Montigaud, B. Tanguy, G. Demazeau, I. Alves, M. Birot, J. Dunogues, Diamond Relat. Mater. 8 (1999) 1707.
[15] J. Ortega, O.F. Sankey, Phys. Rev. B 51 (1995) 2624–2627.
[16] M. Todd, J. Kouvetakis, T.L. Groy, D. Chandrasekhar, S.D. J, P.W. Deal, Chem. Mater. 7 (1995) 1422–1426.
[17] Z. Zhang, K. Leinenweber, M. Bauer, L.A.J. Garvie, P.F. McMillan, G.H. Wolf, J. Am. Chem. Soc. 123 (2001) 7788–7796.
[18] M.J. Bojdys, J.-O. Müller, M. Antonietti, A. Thomas, Chem. Eur. J. 14 (2008) 8177–8182.
[19] J. Sehnert, K. Baerwinkel, J. Senker, J. Phys. Chem. B 111 (2007) 10671–10680.
[20] G. Goglio, D. Andrault, S. Courjault, G. Demazeau, High Pressure Res. 22 (2002) 535–537.
[21] B.V. Lotsch, M. Döblinger, J. Sehnert, L. Seyfarth, J. Senker, O. Oeckler, W. Schnick, Chem. Eur. J. 13 (2007) 4969–4980.
[22] B. Jürgens, E. Irran, J. Senker, P. Kroll, H. Müller, W. Schnick, J. Am. Chem. Soc. 125 (2003) 10288–10300.
[23] T. Komatsu, J. Mater. Chem. 11 (2001) 802–805.
[24] P. Kroll, R. Hoffmann, J. Am. Chem. Soc. 121 (1999) 4696–4703.
[25] D.T. Vodak, K. Kim, L. Iordanidis, P.G. Rasmussen, A.J. Matzger, O.M. Yaghi, Chem. Eur. J. 9 (2003) 4197–4201.
[26] W.C. Kuryla, A.J. Papa, Flame Retardancy of Polymeric Materials, vols. 1–5, Dekker, New York, 1973–1979.
[27] D.R. Miller, D.C. Swenson, E.G. Gillan, J. Am. Chem. Soc. 126 (2004) 5372–5373.
[28] X. Wang, K. Maeda, A. Thomas, K. Takanabe, G. Xin, J.M. Carlsson, K. Domen, M. Antonietti, Nat. Mater. 8 (2009) 76–80.
[29] G.H. Wolf, M. Bauer, K. Leinenweber, L.A.J. Garvie, Z. Zhang, in: H.D. Hochheimer, (Ed.), Frontiers of High Pressure Research II: Application of High Pressure to Low-Dimensional Novel Electronic Materials, Kluwer Academic, The Netherlands, 2001, pp. 29–43.
[30] M. Deifallah, V. Lees, P.F. McMillan, F. Corà, Phys. Rev. B (2009), submitted.
[31] A.C. Ferrari, J. Robertson, Phys. Rev. B 61 (2000) 14095–14107.
[32] A.C. Ferrari, J. Robertson, Phys. Rev. B 64 (2001) 075414.
[33] A.C. Ferrari, J. Robertson, Phil. Trans. R. Soc. Lond. A 362 (2004) 2477–2512.
[34] A.C. Ferrari, S.E. Rodil, J. Robertson, Diamond Relat. Mater. 12 (2003) 905–910.
[35] A.C. Ferrari, S.E. Rodil, J. Robertson, Phys. Rev. B 67 (2003) 155306.
[36] E. Soignard, P.F. McMillan, Chem. Mater. 16 (2004) 3533–3542.
[37] G.R. Loppnow, L. Shoute, K.J. Schmidt, A. Savage, R.H. Hall, J.T. Bulmer, Phil. Trans. R. Soc. Lond. A 362 (2004) 2461–2476.
[38] V.I. Merkulov, J.S. Lannin, C.H. Munro, S.A. Asher, V.S. Veerasamy, W.I. Milne, Phys. Rev. Lett. 78 (1997) 4869–4872.
[39] M. Deifallah, P.F. McMillan, F. Corà, J. Phys. Chem. C 112 (2008) 5447–5453.
[40] P.J. Larkin, M.P. Makowski, N.B. Colthup, Spectrochim. Acta A 112 (1999) 1011–1020.
[41] Y.-L. Wang, A.M. Mebel, C.-J. Wu, Y.-T. Chen, C.-E. Lin, J.-C. Jiang, J. Chem. Soc. Faraday Trans. 93 (1997) 3445–3451.
[42] E. Quirico, G. Montagnac, V. Lees, P.F. McMillan, C. Szopa, G. Cernogora, J.-N. Rouzaud, P. Simon, J.-M. Bernard, P. Coll, N. Fray, R.D. Minard, F. Raulin, B. Reynard, B. Schmitt, Icarus 198 (2008) 218–231.
[43] H. Imanaka, B.N. Khare, J.E. Elsila, E.L.O. Bakes, C.P. McKay, D.P. Cruikshank, S. Sugita, T. Matsui, R.N. Zare, Icarus 168 (2004) 344–366.
[44] R. Livneh, T.L. Haslett, M. Moskovits, Phys. Rev. B 66 (2002) 195110.
[45] D. Lin-Vien, N.B. Colthup, W.G. Fateley, J.G. Grasselli, in: The Handbook of Infrared and Raman Characteristic Frequencies of Organic Molecules, Academic Press, San Diego, 1991.
[46] S. Liu, S. Gangopadhyay, G. Sreenivas, S.S. Ang, H.A. Naseem, Phys. Rev. B 55 (1997) 13020–13024.
[47] N. Mutsukura, K.-I. Akita, Thin Solid Films 349 (1999) 115–119.
[48] N. Gierlinger, C. Hansmann, T. Röder, H. Sixta, W. Gindl, R. Wimmer, Holzforschung 59 (2005) 210–213.
[49] E. Duval, A. Mermet, L. Saviot, Phys. Rev. B 75 (2007) 024201.
[50] G.N. Greaves, F. Meneau, O. Majérus, D. Jones, J. Taylor, Science 308 (2005) 1299–1301.
[51] M. Hass, Solid State Commun. 7 (1969) 1069–1071.
[52] P.F. McMillan, B. Piriou, J. Non-Cryst. Solids 53 (1982) 279–298.
[53] R. Shuker, R.W. Gammon, Phys. Rev. Lett. 25 (1970) 222–225.
[54] P.V. Zinin, L.-C. Ming, S.K. Sharma, V.N. Khabashesku, X. Liu, S. Hong, S. Endo, T. Acosta, Chem. Phys. Lett. 472 (2009) 69–73.